Photo-physical characterization of high triplet yield brominated fluoresceins by transient state (TRAST) spectroscopy

Methods and Applications in Fluorescence

PAPER

Photo-physical characterization of high triplet yield brominated fluoresceins by transient state (TRAST) spectroscopy

Baris Demirbay[1], **Glib Baryshnikov**[2], **Martin Haraldsson**[3], **Joachim Piguet**[1], **Hans Ågren**[4] and **Jerker Widengren**[1,*]

[1] Royal Institute of Technology (KTH), Experimental Biomolecular Physics, Department of Applied Physics, Albanova University Center, SE-106 91, Stockholm, Sweden
[2] Laboratory of Organic Electronics, Department of Science and Technology, Linköping University, SE-60174, Norrköping, Sweden
[3] Chemical Biology Consortium Sweden, Science for Life Laboratory, Department of Medical Biochemistry and Biophysics, Karolinska Institute, SE-171 77 Stockholm, Sweden
[4] Department of Physics and Astronomy, Uppsala University, SE-751 20 Uppsala, Sweden
* Author to whom any correspondence should be addressed.

E-mail: jwideng@kth.se

Keywords: fluorescence, fluorescein, bromination, triplet state, heavy atom effect, intersystem crossing

Supplementary material for this article is available online

OPEN ACCESS

RECEIVED
12 May 2023

REVISED
6 September 2023

ACCEPTED FOR PUBLICATION
19 September 2023

PUBLISHED
3 October 2023

Abstract

Photo-induced dark transient states of fluorophores can pose a problem in fluorescence spectroscopy. However, their typically long lifetimes also make them highly environment sensitive, suggesting fluorophores with prominent dark-state formation yields to be used as microenvironmental sensors in bio-molecular spectroscopy and imaging. In this work, we analyzed the singlet–triplet transitions of fluorescein and three synthesized carboxy-fluorescein derivatives, with one, two or four bromines linked to the anthracence backbone. Using transient state (TRAST) spectroscopy, we found a prominent internal heavy atom (IHA) enhancement of the intersystem crossing (ISC) rates upon bromination, inferred by density functional theory calculations to take place via a higher triplet state, followed by relaxation to the lowest triplet state. A corresponding external heavy atom (EHA) enhancement was found upon adding potassium iodide (KI). Notably, increased KI concentrations still resulted in lowered triplet state buildup in the brominated fluorophores, due to relatively lower enhancements in ISC, than in the triplet decay. Together with an antioxidative effect on the fluorophores, adding KI thus generated a fluorescence enhancement of the brominated fluorophores. By TRAST measurements, analyzing the average fluorescence intensity of fluorescent molecules subject to a systematically varied excitation modulation, dark state transitions within very high triplet yield (>90%) fluorophores can be directly analyzed under biologically relevant conditions. These measurements, not possible by other techniques such as fluorescence correlation spectroscopy, opens for bio-sensing applications based on high triplet yield fluorophores, and for characterization of high triplet yield photodynamic therapy agents, and how they are influenced by IHA and EHA effects.

Abbreviations

AOM	acousto-optical modulator
CFl	carboxy fluorescein
DFT	density functional theory
EHA	external heavy atom effect
FITC	fluorescein isothiocyanate
FCS	fluorescence correlation spectroscopy
FP	flash photolysis
IHA	internal heavy atom effect
ISC	intersystem crossing
KI	potassium iodide
MS	mass spectroscopy
NMR	nuclear magnetic resonance spectroscopy
PCM	polarizable continuum model

PDT	photodynamic therapy
SMD	single molecule detection
SOCME	spin-orbit coupling matrix element
TCSPC	time-correlated single-photon counting
TRAST	transient state spectroscopy/imaging

1. Introduction

Photo-induced dark transient states of fluorophores have been extensively studied for the limitations they set for single molecule fluorescence applications, as well as for their role in enhancing resolution in fluorescence-based super-resolution microscopy [1–3]. Moreover, population dynamics of long-lived, non-fluorescent or weakly fluorescent transient states of fluorophores arising from intersystem crossing [4], trans-cis isomerization [5] or photo-induced charge transfer processes [6] are often highly environment sensitive. This opens for using these states as micro-environmental read-out parameters in bio-molecular research, and to use fluorophores with prominent formation yields of such states. Fluorescent probes with high intersystem crossing (ISC) enable efficient transfer to their lowest triplet state, with possible long lifetime phosphorescence emission [7]. Such fluorophores have found use in several biomedical applications, including photodynamic therapy (PDT) [8, 9], as well as sensing [10] and imaging [11] based on phosphorescence emission. Compared to fluorescence, the phosphorescence signal is however typically weak and strongly compromised by oxygen quenching. ISC can be enhanced by covalent addition of heavy atoms, such as bromine or iodide, yielding an internal heavy atom (IHA) effect by spin–orbit coupling [12, 13]. ISC enhancement can also be effectuated by collisional encounters between heavy atoms and the fluorophores, an external heavy atom (EHA) effect, which is commonly used in fluorescence spectroscopy to get insights about molecular interactions [13]. IHA and EHA effects have been largely studied by transient absorption spectroscopy (or flash photolysis, FP) [14, 15], with transient states monitored via their absorption by a separate probing beam, following an excitation pulse. However, FP is technically relatively complicated, lacks the sensitivity for measurements at low ($<\mu$M) concentrations, and absorption spectra of transient states can overlap and thus be difficult to spectrally separate from each other. Moreover, while the decay of the transient state absorption can be followed, it is more complicated to determine the absolute rates of formation of the transient states. Transient dark state transitions in fluorophores can also be followed via fluorescence-based single molecule detection (SMD) methods, in which fluorophore blinking behavior can be monitored on the fly, without need of synchronization. However, SMD requires high brightness fluorophores, which typically makes fluorophores with prominent triplet quantum yields too dim to be properly analyzed. Moreover, their singlet–triplet state transitions typically take place at sub-microsecond time scales. This is typically too fast and generates too few photons within the event to be properly analyzed on a single molecule level. Compared to SMD methods, fluorescence correlation spectroscopy (FCS), analyzing fluorescence intensity fluctuations of larger numbers of single fluorophores on a cumulative, ensemble level, offers extended possibilities to analyze transient dark states of fluorophores, such as singlet–triplet [16], isomerization [17, 18] and photo-induced charge transfers [19]. On these premises, FCS was used to investigate EHA effects of potassium iodide (KI) under typical excitation conditions for SMD, and where it was found that KI can function both as a fluorescence quencher and promoter [3, 20]. However, as a method relying on SMD conditions, also FCS measurements ultimately depend on the molecular brightness of fluorophores, and the higher their triplet quantum yield, the lower their fluorescence brightness, and the more challenging it is to analyze their singlet–triplet transitions. Increasing the excitation intensity can lead to higher fluorophore brightness, but fluorescence saturation due to triplet state buildup sets a limit for this gain. With the relaxation time for this buildup then also moved into shorter time ranges, it may even overlap with the antibunching relaxation of the fluorophores [21], and signal-to-noise conditions in the recorded FCS curves are further compromised [22]. Moreover, the contribution of a fluorescent species to a recorded FCS curve scales with its molecular brightness squared. With a typically non-uniform excitation intensity within the detection volume used in FCS experiments, the contribution from different parts of the detection volume can strongly vary depending on the degree of dark state build-up/saturation [16], which further complicates analyses of high triplet yield fluorophores. Thus, both SMD methods and FCS possess limitations in resolving the higher ISC rates of heavy atom-containing fluorophores. Transient state (TRAST) monitoring offers a means to circumvent many of these limitations and allows transient state dynamics of fluorophores to be followed in a widely applicable manner [3, 23].

TRAST analyses the time-averaged fluorescence intensity, $\langle F_{exc}(w)\rangle$, detected from fluorophores subject to a modulated excitation. With the modulation systematically varied over the time range of the dark state transitions of the fluorophores, these transitions can be determined form how $\langle F_{exc}(w)\rangle$ varies with the modulation characteristics [6, 24–27]. The TRAST method does not rely on SMD conditions nor on a

high time resolution in the detection, as needed for FCS. This makes it possible to extend dark state transition studies in fluorophores to more demanding samples with limited signal-to-background conditions, to fluorophores with lower brightness, including autofluorescent compounds [27–29], and allow investigations under far lower excitation intensities than used in FCS experiments. Heavy atom substitution by e.g. bromines offers a means to enhance triplet state formation by an IHA effect. Thereby, prominent triplet state populations can be reached also under moderate excitation intensities, which offers an advantage in live cell TRAST and phosphorescence studies. Yet, brominated fluoresceins, such as e.g. Eosin, are also broadly used as fluorophores in cellular imaging, in which case triplet state formation rather constitutes a limiting factor. In this work, we applied wide-field TRAST spectroscopy to study the overall effects of heavy ions on the photo-physics of carboxy-Fluorescein (CFl) and three synthesized CFl derivatives, with different numbers of bromine atoms. We investigated how triplet state transition and photo-oxidation rate parameters varied with the number of bromines attached on the common CFl body, and how EHA effects mediated by potassium iodide (KI) added into the fluorophore solutions were manifested. We found that the intrinsic ISC rate dramatically increased by the number of covalently added bromines, and with increasing KI concentrations. Interestingly, at the same time addition of KI leads to an overall reduction in the triplet state populations of the brominated fluorophores. By enhancing not only the ISC rates, but also the triplet decay rates, iodine ions can act as a net fluorescence promoter for these fluorophores, as opposed to bromine-free CFl. The TRAST experiments were complemented with density functional theory (DFT) calculations, suggesting that for the observed, high ISC rates to be generated in the fluorophores, ISC may have to take place to a higher triplet state, from which relaxation to the lowest triplet state then takes place. Fluorescein fluorophores, and brominated variants such as Eosin, are broadly used as labels of molecules, cells and tissues. Apart from a typical pH sensitivity, rendering them suitable as pH sensors [13], modified fluoresceins have also found use for lifetime-based sensing [30]. In lifetime-based sensing, quenching needs to be effectuated in the time range (ns) of the excited singlet state (S_1) lifetime to be properly detected [13]. If instead the quenching of more long-lived photoinduced states, such as triplet (T) and photo-oxidized ($\dot{R}^+$) states, can be monitored then also more rare and lower frequency interactions can be detected [6, 31]. Taken together, the TRAST experiments show that dark state transitions within high triplet yield fluorophores can be readily analyzed, and that IHA and EHA effects can be followed, also in e.g. biological samples not amenable to SMD- , FCS- or FP-based analyses. By use of high-triplet yield fluorophores, prominent triplet state populations can be generated also at moderate excitation intensities, minimizing possible photo-toxic effects. This offers a promising basis for bio-imaging of high triplet yield fluorophores, as well as for characterization of high triplet yield PDT agents, for local monitoring of their therapeutic effects via their ISC rates.

2. Materials and methods

2.1. Fluorophore synthesis and sample preparation

Four carboxy-Fluoresceins were synthesized without bromination, or with a mono-, di- and tetra-bromination (figures 1(a)–(d)). The synthesis of CFl and the corresponding brominated fluorophores (CFl-Br, CFl-2Br and CFl-4Br) and the subsequent verification by nucleic magnetic resonance (NMR) and mass spectrometry (MS) are further described in the Supplementary part, sections S4 and S5. Fluorescein-5-isothiocyanate (FITC, Thermo Fisher Invitrogen, Cat. No: 143)) was used without further purification. Aliquoted fluorophore stock solutions (100 μM) in phosphate-buffered saline (PBS, pH = 7.4) were prepared from powder samples, stored in freezer at −20 °C, then thawed and diluted in PBS to a final concentration of 100 nM before experiments. Potassium iodide (KI, Sigma Aldrich) was added in concentrations up to 50 mM in the diluted samples. The pH of all measured samples were set at 9.3, to eliminate any pH dependent effects and to keep the fluorophores in a fluorescent deprotonated state (pK_a of ∼6.5 [32]).

2.2. TRAST spectroscopy

2.2.1. Theoretical concept and photophysical model

In TRAST spectroscopy, photo-induced blinking kinetics of fluorescent molecules are studied via the time-averaged fluorescence intensity from samples under a modulated excitation scheme, varied on the time scales of the dark state transitions underlying the blinking [3, 25]. Blinking kinetics occuring in a μ s-ms time range can then be quantified without the need for time-resolved detection. To calculate the fluorescence intensity in the TRAST experiments, we used a common photo-physical model for all fluorophores, including a ground singlet state, S_0, an emissive, excited singlet state, S_1, a dark triplet state, T, and a dark photo-oxidized radical state, $\dot{R}^+$, (figure 2). This model corresponds to previously used models for similar xanthene fluorophores [20, 24], but due to the lower excitation rates applied in this work, population of higher excited singlet and triplet states can be disregarded. For a fluorescent molecule subject to a rectangular excitation pulse initiated at $t = 0$, the resulting detected fluorescence intensity can then be given by

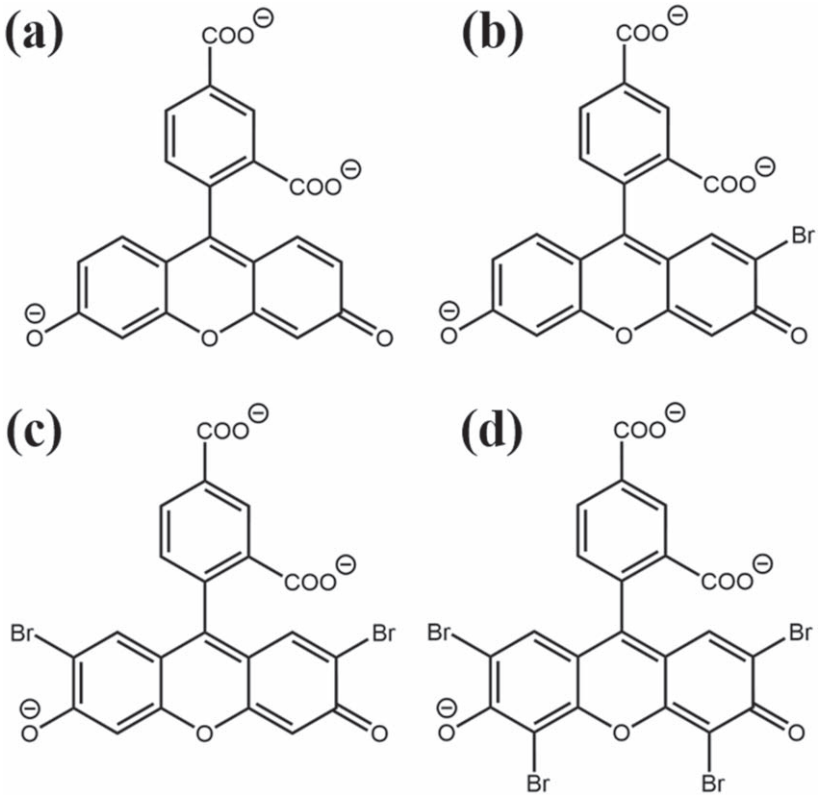

Figure 1. Molecular structures of (a) carboxy-Fluorescein (CFl), (b) mono-bromo carboxy-Fluorescein (CFl-Br), (c) di-bromo carboxy-Fluorescein (CFl-2Br) and (d) tetra-bromo carboxy-Fluorescein (CFl-4BR). All fluorophores are shown in their quinoid tri-anion states, the dominant forms at pH = 9.3 [33], as used in this work for the spectroscopic measurements.

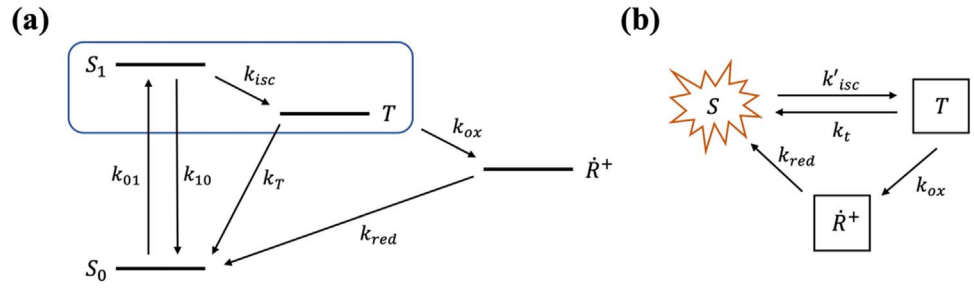

Figure 2. (a) Electronic state model used in this work for CFl and brominated CFl derivatives. S_0 and S_1 denote the ground and first excited singlet states , with k_{01} and k_{10} representing the excitation and de-excitation rates, respectively. k_{isc} denotes the intersystem crossing rate from S_1 to the triplet state, T, and k_T the triplet decay rate back to S_0. Photo-oxidation of fluorophores to $\dot{R}^+$ state is assumed to occur from both S_1 and T, with a rate denoted k_{ox}. From the long-lived $\dot{R}^+$ state, the fluorophores can relax back to S_0 through a photo-reduction rate, k_{red}. (b) Simplified electronic three-state model, describing state transitions taking place on a time scale much longer than the equilibration of the S_0 and S_1 states, where S represents both these singlet states and $k'_{isc} = \frac{k_{01}}{k_{01}+k_{10}} k_{isc}$. Since the singlet–triplet state transitions are much faster, the S and T populations are equilibrated on the timescale of the transitions to and from $\dot{R}^+$. We can then for simplicity assume photo-oxidation to take place only from T.

$$F(t) = c q_f q_D \int\int\int \frac{k_{01}(\bar{r})}{k_{01}(\bar{r}) + k_{10}} S(\bar{r}, t)\, CEF(\bar{r})\, dV \quad (1)$$

where c is the fluorophore concentration, q_f is the fluorescence quantum yield, q_D denotes the overall detection quantum yield of the microscope, $CEF(\bar{r})$ represents the collection efficiency function and $S(\bar{r}, t)$ the probability that a fluorophore, residing at position $\bar{r}$ in the detection volume, is in either its ground (S_0) or excited (S_1) singlet state at time t. $k_{10} = 1/\tau_f - k_{isc} - k_{ox}$ denotes the decay rate within the fluorophores from S_1 to S_0, $k_{01} = \sigma_{exc}\Phi_{exc}(\bar{r}) = \sigma_{exc} I_{exc}(\bar{r})/h\nu$ represents the excitation rate from S_0 to S_1, where σ_{exc} is the excitation cross section of the fluorophore, $\Phi_{exc}(\bar{r})$ the local excitation flux, $I_{exc}(\bar{r})$ the excitation intensity and $h\nu$ is the excitation photon energy [27]. With a constant excitation starting at $t = 0$, the probability for a fluorophore to be in a singlet state (S_1 or S_0) at time t can in a general form be described by:

$$S(t) = 1 - \sum_{i=1}^{p}[A_i - A_i e^{-\lambda_i t}] \quad (2)$$

Here, λ_i are the eigenvalues, i.e. the rates of relaxation modes of $S(t)$ upon onset of constant excitation, and A_i the related amplitudes, reflecting the population build-up of the different photo-induced non-fluorescent states at steady-state ($t \gg 1/\lambda_i$). With a suitable initial condition, typically $S(0) = 1$, λ_i and A_i can be described analytically. At onset of excitation, equilibration between the S_1 and S_0 states takes place within the fluorescence lifetime (ns), with the so-called anti-bunching relaxation time ($\tau_{ab} = 1/(k_{01} + k_{10})$) [21]. This relaxation is typically averaged out on the time scales of the dark state transitions monitored by TRAST, and we can thus reduce our photophysical model of figure 2(a), to three states (figure 2(b)); the fluorescent S (S_1 and S_0), and the non-fluorescent T and $\dot{R}^+$ states, and with characteristic relaxations in timescales of μ s to ms of $S(t)$ and $F(t)$, attributed to build-up of T and $\dot{R}^+$ state populations (corresponding rate equations and their analytical solution are given in section S1). This relaxation process is also reflected in the time-averaged fluorescence signal generated by a rectangular pulse with a duration of w:

$$\langle F_{exc}(w)\rangle = \frac{1}{w}\int_0^w F(t)\,dt \quad (3)$$

where the change of $\langle F_{exc}(w)\rangle$ with w allows the population kinetics of long-lived, dark transient states, such as T and $\dot{R}^+$, to be determined, which is the general basis for TRAST method. So-called TRAST curves are then generated by collecting $\langle F_{exc}(w)\rangle$ over multiple pulses, M, for different pulse durations, w, normalized by $\langle F_{exc}(w)\rangle$ recorded with a pulse train with short pulse duration, w_0:

$$\langle F_{exc}(w)\rangle_{norm} = \left(\frac{1}{M}\sum_{i=1}^{M} F_{exc}(w)_i\right) \Big/ \left(\frac{1}{M_0}\sum_{i=1}^{M_0} F_{exc}(w_0)_i\right) \quad (4)$$

Here, w_0 is selected to be short enough to avoid the build-up of dark transient states ($w_0 \ll 1/\lambda_i$), yet longer than the anti-bunching relaxation time ($w_0 \gg \tau_{ab}$). By this normalization, the terms, c, q_D and q_f (equation (1)) cancel out. Moreover, at low duty cycles of the excitation pulse trains, allowing the dark transient states of the fluorescent molecules to completely relax back to the singlet ground state, S_0, before the onset of next excitation pulse, all generated pulses in the pulse train can be treated as identical. We can then write:

$$\langle F_{exc}(w)\rangle_{norm} = \frac{1}{M}\sum_{i=1}^{M}\left(\frac{1}{w}\int_w^0 S(t)\,dt\right)_i = \frac{1}{w}\int_0^w S(t)\,dt \quad (5)$$

2.2.2. Experimental setup

Wide-field TRAST measurements were performed on an inverted, wide-field epi-fluorescence microscope setup (figure 3), based on a stand from Olympus (IX73). For excitation, a continuous wave (CW) 488 nm diode laser (Cobolt, 06-MLD, max. output power: 200 mW) was used with an excitation filter (BrightLine 488/10, Semrock). The CW excitation beam was modulated by an acousto-optic modulator (AOM, AA Opto Electronics, MQ180-A0,25-VIS) to generate rectangular excitation pulse trains with different pulse durations (between 100 ns and 1 ms). The beam was then reflected by a dichroic mirror (FF506-Di03, Semrock) and focused to the back aperture of a water-immersion microscope objective (Olympus, UPLSAPO 60x/NA1.20) to generate a wide-field illumination with a beam waist of $\omega_0 = 18\,\mu$m ($1/e^2$ radius) in a sample plane. The fluorescence signal from the sample was collected by the same objective, transmitted through the dichroic mirror and an emission filter (BrightLine 530/55, Semrock), and was then detected by an sCMOS camera (Hamamatsu, ORCA-Flash4.0 v2). The duty cycle of the excitation pulse trains was kept low, $\eta = 0.01$, to allow the fluorophores in the sample to fully recover back to S_0 before the onset of the next pulse. To obtain sufficient photon counts, even for short w, the number of identical pulse repetitions in each excitation pulse train, M (equation (4)), was adjusted to maintain a constant laser illumination time, $t_{ill} = M \cdot w$,c for all w, and with t_{ill} kept at 10 ms. The AOM operation and the TRAST measurements were controlled by a custom software developed in Matlab environment and by use of a digital I/O card (from National Instruments, PCI-6602) [26].

2.2.3. Wide-field TRAST data analysis

The experimental TRAST curves (equation (4)) were obtained from a stack of 30 fluorescence images, where each image was recorded over an entire excitation pulse train with a certain $\boldsymbol{w}$. Pulse trains with different pulse durations were applied, with $\boldsymbol{w}$ distributed logarithmically between 100 ns and 1 ms, and measured in a randomized order to avoid bias due to time effects. An additional 10 reference frames, all using 100 ns pulse duration to avoid dark state build-up, were inserted at regular intervals between the 30 main images to track any permanent bleaching of the sample. The overall observed bleaching was typically 5%–10% of the total detected intensity in the measurements. Prior to analysis, the recorded TRAST data was first pre-processed by subtraction of the static ambient background. In all measurements, TRAST curves were produced by recording $\langle F_{exc}(w)_{norm}\rangle$ within a region of interest (ROI) corresponding to a 13 μm radius in the sample plane, centered on the excitation beam. Fitting of photophysical rate parameters was then performed following the same general procedure as previously described [27], here specifically simulating theoretical TRAST curves using equations (1)–(5) and based on the photophysical model of figure 2(b), and then comparing these curves to the experimental data. The set of rate parameter values best describing the experimental data was then found using non-linear

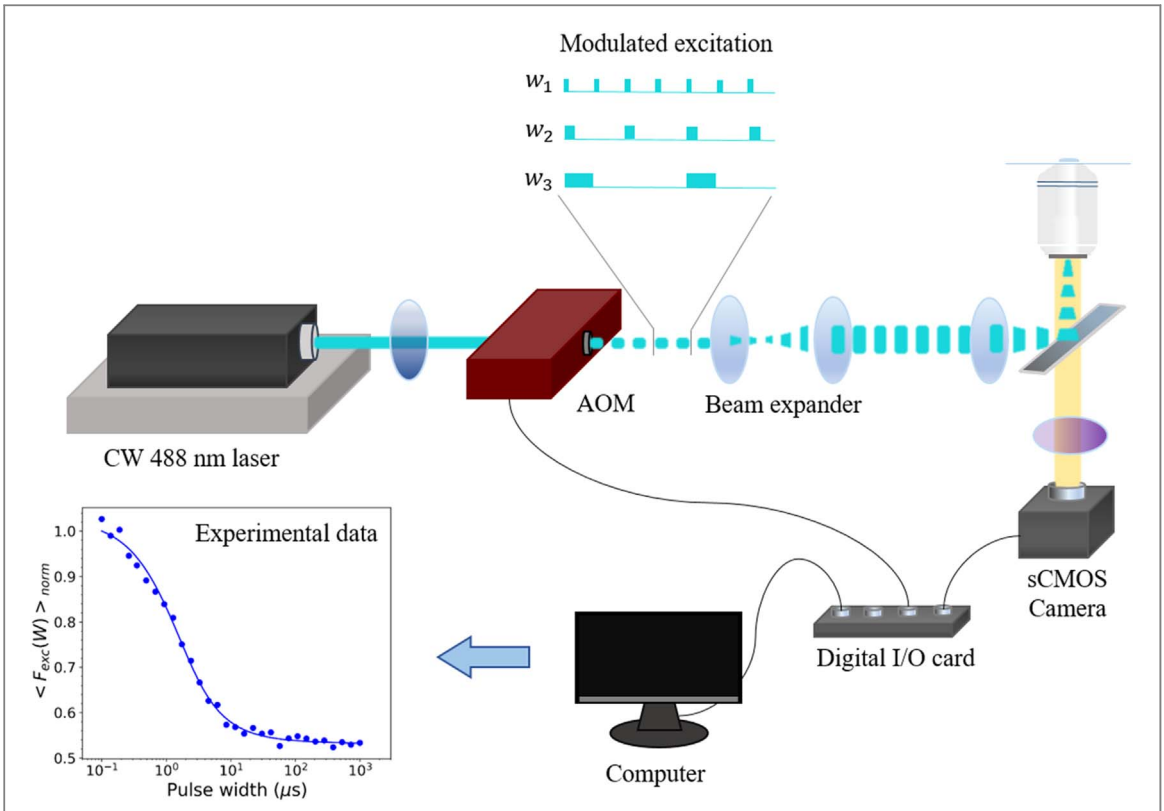

Figure 3. Visual representation of the wide-field TRAST setup used in this study (see main text for details).

least squares optimization. In the fitting of the TRAST curves, the excited state lifetime for each fluorophore, τ_f, was fixed to a value determined by time-correlated single photon counting (TCSPC) measurements (described in section 2.3 below), and with $1/\tau_f$ comprising all deactivation (including ISC) rates from S_1. Moreover, an average singlet excitation rate, $\hat{\boldsymbol{k}}_{01}$, was calculated for each ROI using equation (S5) (see [27] or Supplementary section S2 for details).

2.3. Fluorescence lifetime measurements

TCSPC measurements were performed with a pulsed excitation beam of a diode laser (485 nm, Picoquant GmbH, LDH-D-C-485) fed into an inverted, epi-illuminated confocal microscope (Olympus FV1200) with a water immersion objective (60x, NA1.2, Olympus, UPlanSApo). The fluorescence was collected by the same objective, passed through a dichroic mirror (ZT405/473–491/NIRrpc-UF2, Chroma) and an emission filter (HQ535/70, Chroma) and then recorded by single photon counting avalanche photodiodes (Perkin & Elmer, SPCM-AQR-14). The signals were fed into a data acquisition card (Hydraharp, Picoquant GmbH), deconvoluted and then fit to an exponential decay based on non-linear least squares minimization (Symphotime, Picoquant GmbH). Deconvolution was based on an instrument response function (IRFs) determined from the back-reflected light from the laser excitation pulses.

2.4. Absorption and fluorescence emission spectra measurements

Absorption spectra of the fluorophores (1 μM, PBS, pH = 9.3) were recorded in cuvettes by a spectrophotometer (UV5, Mettler Toledo), corrected for the spectral response of the instrument, and with background contributions subtracted using blank PBS solutions. Emission spectra were recorded by a spectrofluorometer (FluoroMax-3, HORIBA), using an excitation wavelength of 488 nm and a 1 nm band-pass slit.

2.5. Density functional theory (DFT) calculations

To further investigate the IHA effects for the different fluorophores (CFl, CFl-Br, CFl-2Br and CFl-4Br), quantum-chemical estimations of the main photophysical rate parameters (the radiative rate from the S_1 state, k_r, and the ISC rate, k_{isc}) were performed at different levels of density functional theory (DFT), and employing a polarizable continuum model (PCM) to take solvent effects into account. Computational details for these quantum chemical estimations are given in the Supplementary part S3.

3. Results and discussion

3.1. Fluorescence lifetime and spectrometer measurements

CFl and mono-, di- and tetra-brominated forms of CFl (CFl-Br, CFl-2Br and CFl-4Br) were synthesized

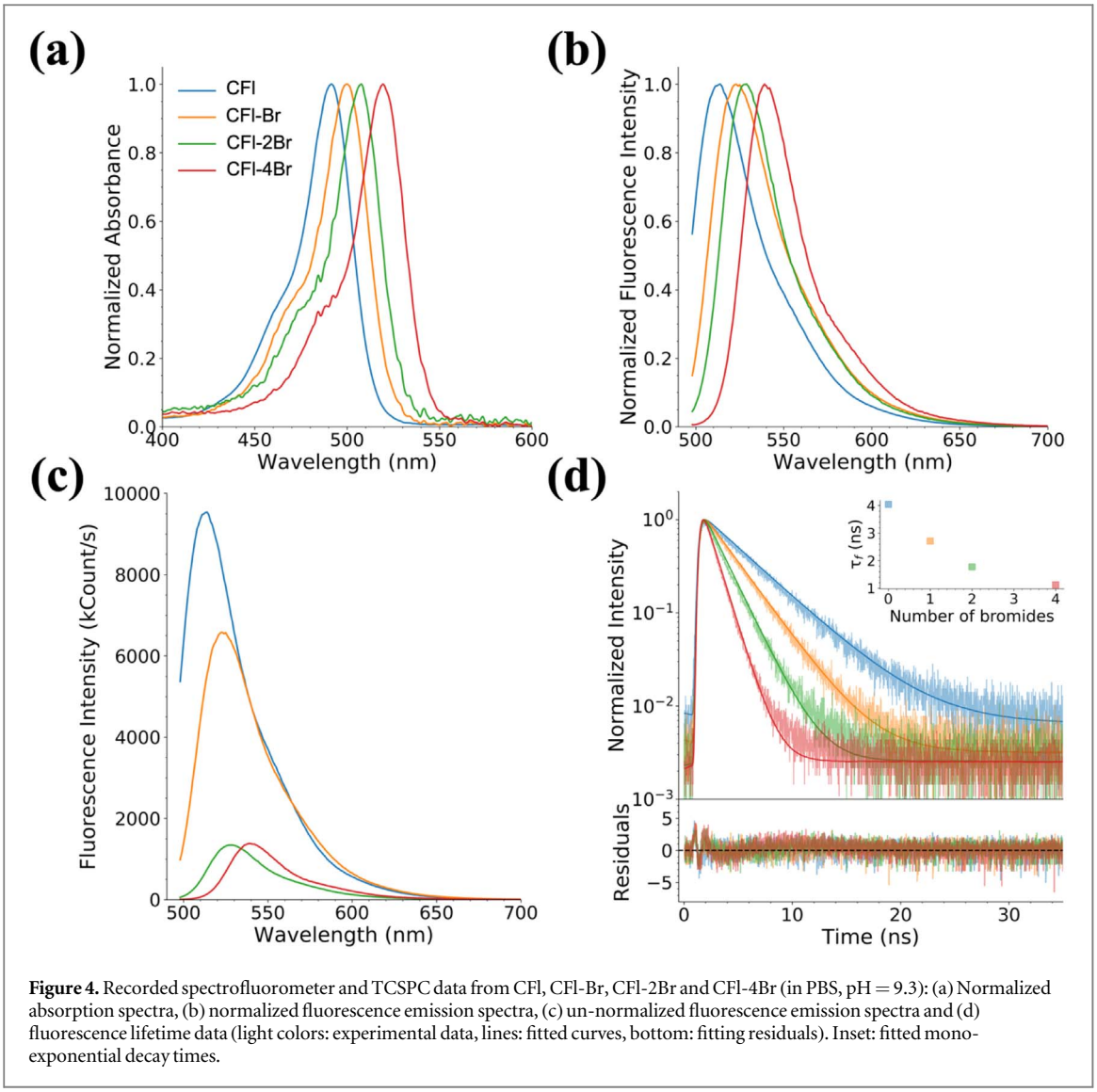

Figure 4. Recorded spectrofluorometer and TCSPC data from CFl, CFl-Br, CFl-2Br and CFl-4Br (in PBS, pH = 9.3): (a) Normalized absorption spectra, (b) normalized fluorescence emission spectra, (c) un-normalized fluorescence emission spectra and (d) fluorescence lifetime data (light colors: experimental data, lines: fitted curves, bottom: fitting residuals). Inset: fitted mono-exponential decay times.

Table 1. Fluorescence lifetimes, τ_f, estimated σ_{exc} at 488 nm, relative fluorescence intensities and peak absorption and emission wavelengths for CFl and its brominated derivatives.

Fluorophore	σ_{exc}(488 nm)(10^{-16} cm^2)	τ_f(ns)	Relative fluorescence intensity	Absorption peak wavelength		Emission peak wavelength	
				(nm)	(eV)	(nm)	(eV)
CFl	3.00	4.04	1.00	492	2.52	513	2.42
CFl-Br	2.52	2.71	0.69	500	2.48	523	2.37
CFl-2Br	1.77	1.77	0.141	507	2.45	529	2.34
CFl-4Br	1.65	1.12	0.145	519	2.39	540	2.30

and characterized by NMR and MS (described in Supplementary, section S4), dissolved in PBS (pH 9.3, 100 nM), and then characterized by TCSPC and spectrometer measurements, as described in Methods and Materials. Both the absorption and fluorescence emission spectra displayed a clear red shift with higher degree of bromination of the fluorophores (figures 4(a) and (b)). Such red shift has been previously reported and has been explained by quantum chemical calculations to be due to charge redistributions upon halogenation [34] and can also be inferred from our DFT calculations (see section 3.3 below). The fluorescence intensities for the different fluorophores were also found to decrease with higher degree of bromination (figure 4(c), table 1). Shorter fluorescence lifetimes were also recorded with higher degree of bromination of the fluorophores (figure 4(d)). This together indicates that

non-radiative rates from the excited singlet state of the fluorophores are enhanced with the degree of bromination, likely as a result of an IHA effect. The fluorescence decay curves could be well fitted to a mono-exponential decay (decay times listed in figure 4(d), inset). Fitting to a two-exponential decay model did not yield better fitting results (data not shown), consistent with an IHA effect, and giving no evidence of any additional emitting species in the brominated fluorophores.

The excitation cross sections, σ_{exc}, at 488 nm, the excitation wavelength used in the TRAST experiments, were set to $\sigma_{exc} = 3 \cdot 10^{-16}$ cm^2 for CFl (at 488 nm) [35], while the σ_{exc} values for the other three fluorophores were estimated from a reported peak $\sigma_{exc} = 3.7 \cdot 10^{-16}$ cm^2 for CFl-4Br [36], with σ_{exc} for CFl-Br and CFl-2Br assumed to have the same peak σ_{exc} as CFl-4Br. The resulting estimated σ_{exc} values at 488 nm excitation are listed in table 1, together with the peak absorption and emission wavelengths, and the relative fluorescence intensities of the different fluorophores.

3.2. Transient state (TRAST) spectroscopy measurements

Wide-field TRAST measurements were performed on the fluorophores (CFl, CFl-Br, CFl-2Br and CFl-4Br, 100 nM) in PBS (pH 9.3), as described in Materials and Methods. In the recorded TRAST curves, a prominent relaxation was observed in the microsecond time range, which increased amplitude with higher degree of bromination of the fluorophores (figure 5(a)). This is consistent with triplet state formation and an IHA effect, promoting the k_{isc} rates of the fluorophores. This promotion was found to be significant also for the mono-brominated fluorophore (CFl-Br). On a slower, sub-millisecond, time scale a second relaxation process could be observed in the TRAST curves, most prominent for the non-brominated fluorophore (CFl). We attribute this relaxation to photo-oxidation, as has been previously observed for e.g. rhodamine fluorophores in FCS [20] and TRAST [37] experiments, and consistent with the photophysical model of figure 2.

We then recorded TRAST curves from CFl at different excitation intensities (figure 5(b)), which were globally fitted to the model of figure 2 (procedure described in Methods and Materials). In the fit, $\boldsymbol{\sigma_{exc}}$ and k_{10} were fixed to $3 \cdot 10^{-16}$ cm^2 and to $1/\boldsymbol{\tau_f} = 250 \times 10^6$ s^{-1}, respectively, as determined from the spectrofluorometer and TCSPC measurements (table 1), while k_{isc}, k_T, k_{ox} and k_{red} were fitted as global parameters. The fitted curves could well reproduce the experimental data, with fitted parameter values in reasonable agreement with previously reported values [16]. The fitted values are listed in the caption of figure 5(b), and in table 2.

Next, we studied effects upon adding potassium iodide (KI), known to act as a fluorescence quencher via an EHA effect, by dynamic quenching upon collisional encounters of the I^- ions with the fluorophores [13]. Depending on the conditions, however, iodide can act both as a fluorescence quencher and a promoter. In FCS experiments on rhodamine fluorophores with similar excitation and emission spectra as the fluorophores studied here, KI has been found not only to enhance k_{isc} by an EHA effect, but also to enhance their k_T rates by a charge-coupled deactivation, as well as to act as an antioxidant, promoting the recovery of photo-oxidized fluorophores [20]. However, in contrast to the trend observed for the rhodamine fluorophores in [20] (Rhodamine green, RhGr), the triplet relaxation amplitude for CFl was found to increase with higher KI concentrations, [KI] (figure 4(c)). For the brominated, CFl-Br, CFl-2Br and CFl-4Br fluorophores, however, a reduction in the triplet state amplitude (or build-up) was observed with higher [KI] (figures 5(d)–(f)). The recorded TRAST curves in figures 5(c)–(f) were fitted in a similar way as the curves in figure 5(b), with σ_{exc} and k_{10} fixed to the values determined from the spectrofluorometer and TCSPC measurements (table 1) and using the same model (figure 2). In the fits, we also introduced a linear dependence on [KI] for the k_{isc}, k_T and k_{red} rates, as found previously for rhodamine fluorophores [20]:

$$k_{isc} = k_{isc}^0 + k_{Qisc} \cdot [KI] \quad (6A)$$

$$k_T = k_T^0 + k_{QT} \cdot [KI] \quad (6B)$$

$$k_{red} = k_{red}^0 + k_{Qred} \cdot [KI] \quad (6C)$$

In the fits the rates at [KI] = 0 mM, k_{isc}^0, k_T^0 and k_{red}^0, as well as the KI enhancement pre-factors, k_{Qisc}, k_{QT} and k_{Qred}, were all fitted as global parameters for the set of eight TRAST curves recorded (for [KI] between 0 and 50 mM) for each fluorophore. The resulting sets of fitted curves could well reproduce the experimental TRAST curves for all the fluorophores (figures 5(c)–(f)). The fitted parameter values are plotted in figures 6(a)–(d) and summarized in table 2.

KI has previously been found to generate two major effects on the triplet state kinetics of xanthene fluorophores [20]. On the one hand, the k_{isc} rates are significantly enhanced by an EHA effect. This EHA effect, given by k_{Qisc} in equation (6A), was found to be quite similar for CFl, CFl-Br, CFl-2Br and CFl-4Br, compared to previously reported k_{Qisc} [20]. Additionally, for fluorophores with an excitation maximum in the blue spectral range, a KI-mediated charge-coupled deactivation of their triplet states can also take place, indicating that the triplet state energies of these fluorophores lie above a threshold level, above which deactivation by an electron exchange reaction with KI is possible [20]. Consequently, addition of KI can have opposite effects on different fluorophores, on the one hand strongly promoting triplet state formation in xanthene fluorophores in the green-red spectral range, while even diminishing triplet state populations in corresponding fluorophores in the blue spectral range.

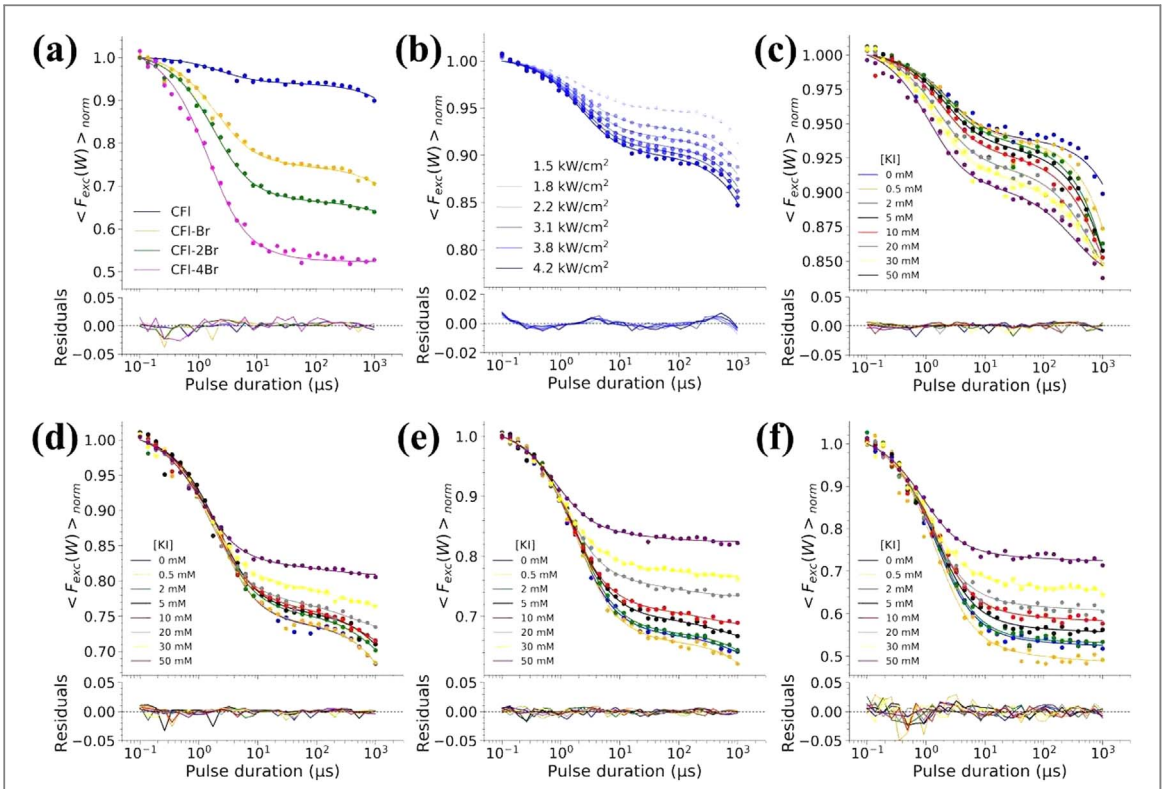

Figure 5. Fitted (lines) and experimental (dots) TRAST curves recorded from 100 nM fluorophore solutions (1.2 mM PBS, pH = 9.3). Fitting residuals plotted below. TRAST curves measured with $I_{exc} = 1.5$ kW cm^{-2}, if not otherwise stated. (a) Comparison of TRAST curves recorded from CFl, CFl-Br, CFl-2Br and CFl-4Br solutions. (b) TRAST curves recorded from a CFl solution with different I_{exc} applied (inset). Global fitting of the curves, with k_{isc}, k_T, k_{red} and k_{ox} fitted as global parameters, yielded: $k_{isc} = 9.14\ \mu s^{-1}$, $k_T = 0.71\ \mu s^{-1}$, $k_{red} = 0.00001\ \mu s^{-1}$ and $k_{ox} = 0.00098\ \mu s^{-1}$. (c)–(f) TRAST curves recorded from CFl (c), CFl-Br (d), CFl-2Br (e) and CFl-4Br (f) solutions with different [KI] (0–50 mM). The curves were fitted globally, as described in the main text. The resulting fitted parameters listed in table 2.

Table 2. Globally fitted rates from the TRAST curves shown in figures 5(c)–(f). The uncertainties refer to the 95% confidence intervals obtained from the fitting of the TRAST curves.

Fluorophore	$k_{Qisc}(10^9\,M^{-1}s^{-1})$	$k^0_{isc}\ (\mu s^{-1})$	$k_{QT}(10^8\,M^{-1}s^{-1})$	$k^0_T\ (\mu s^{-1})$	$k_{Qred}(10^6\,M^{-1}s^{-1})$	$k^0_{red}(s^{-1})$
CFl	$0.52 \pm 18\%$	$10.8 \pm 10\%$	$0.13 \pm 5\%$	$0.70 \pm 11\%$	$0.10 \pm 21\%$	$10 \pm 27\%$
CFl-Br	$0.52 \pm 20\%$	$94.5 \pm 4\%$	$0.11 \pm 20\%$	$0.61 \pm 5\%$	$0.15 \pm 8\%$	$10.4 \pm 9\%$
CFl-2Br	$0.54 \pm 20\%$	$309 \pm 3\%$	$0.18 \pm 12\%$	$0.61 \pm 3\%$	$0.48 \pm 9\%$	$0.47 \times 10^3 \pm 4\%$
CFl-4Br	$0.24 \pm 11\%$	$893 \pm 5\%$	$0.16 \pm 21\%$	$0.58 \pm 6\%$	$0.47 \pm 4.2\%$	$5 \times 10^3 \pm 2\%$B
RhGr [20]	0.60	1	7	0.4	—	—
FITC [16]	—	$5.7 \pm 30\%$	—	$0.48 \pm 10\%$	—	—
FITC[a]	$0.68 \pm 12\%$	$9.64 \pm 12\%$	$0.12 \pm 2\%$	$0.72 \pm 10\%$	$0.10 \pm 25\%$	$10 \pm 32\%$

[a] Corresponding TRAST measurements presented in SI, section S6 (figure S1).

CFl deviates from this 'spectral rule', showing an increased triplet state population with higher [KI] (figure 5(c)). A likely reason is that CFl is negatively charged, making close collisional encounters and triplet state deactivation by charge transfer between CFl and I^- less probable than in zwitterionic or positively charged (RhGr) fluorophores. Indeed, the k_{QT} quenching coefficient for CFl, CFl-Br, CFl-2Br and CFl-4Br was found to be about two orders of magnitude lower than for RhGr [20], although the fluorophores are in the same blue spectral range. Similarly, k_{Qred} was found to be orders of magnitude lower for CFl, CFl-Br, CFl-2Br and CFl-4Br than in RhGr (table 2), which reflects that these, all negatively charged fluorophores are far less likely than RhGr to accept an electron from I^- upon collisional encounter. In contrast to CFl, the brominated fluorophores showed a significant decrease in their triplet state populations with increasing [KI] (figures 5(d)–(f)), although very similar k_{Qisc} and k_{QT} coefficients were found for these fluorophores. This is, however, to be expected since the measured triplet state populations depend on the ratio k_{isc}/k_T. For the brominated fluorophores, but not for CFl, the relative increase of k_{isc} is lower than the relative increase of k_T, and the k_{isc}/k_T ratio then decreases with higher [KI]. For reference, we also studied the photodynamics of Fluorescein 5-Isothiocyanate (FITC) and its dependence on Φ_{exc}

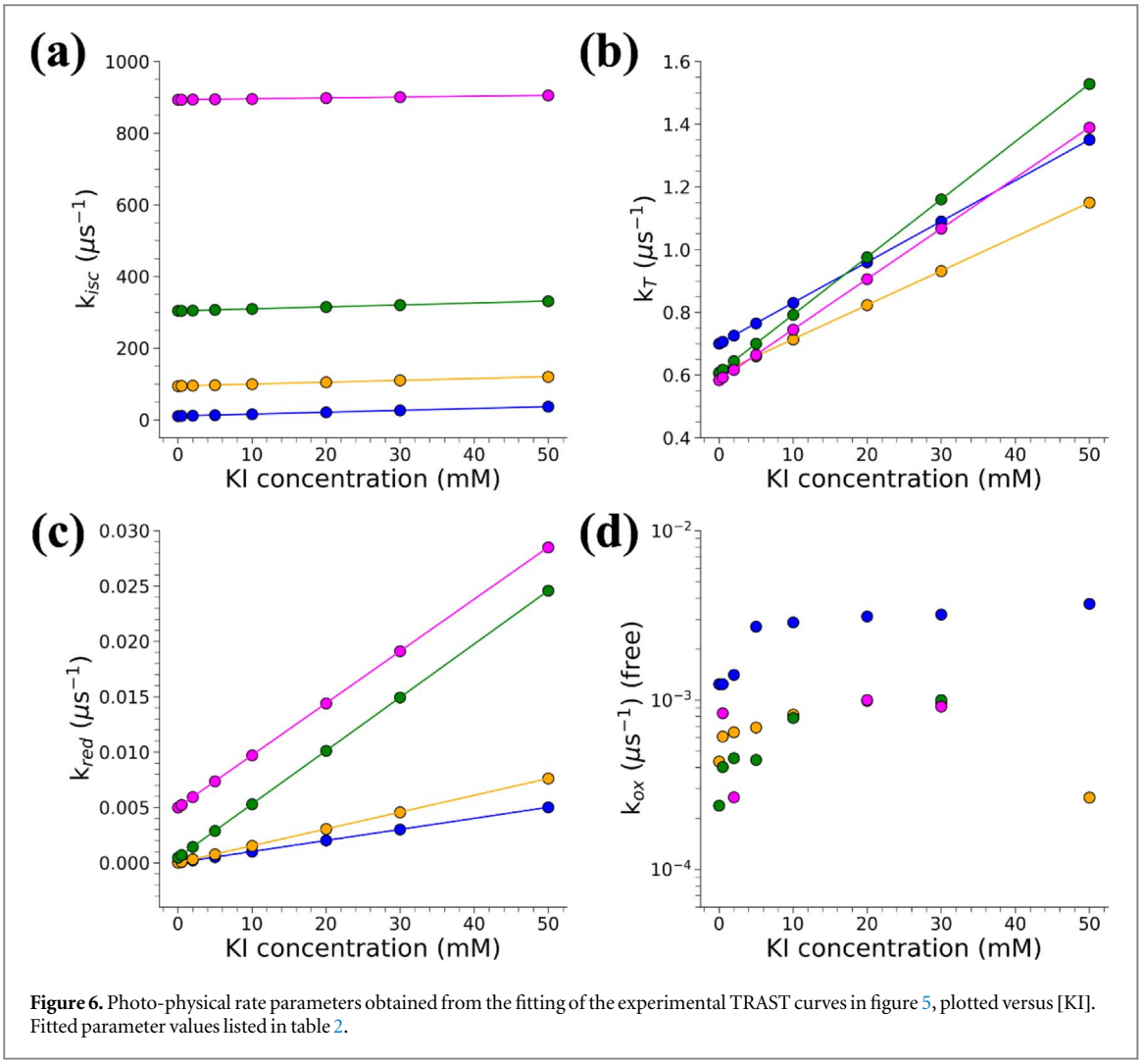

Figure 6. Photo-physical rate parameters obtained from the fitting of the experimental TRAST curves in figure 5, plotted versus [KI]. Fitted parameter values listed in table 2.

and [KI] under the same conditions as for the other fluorophores (experimental and fitted TRAST curves presented in SI, section S6, figure S1). As for CFl, we also observed an increase in the triplet state buildup for FITC with higher [KI], which can be explained by the negative charge of FITC (di-anion at pH 9.3). Also, the singlet–triplet and redox kinetics were very similar to those of CFl (table 2), which indicates that alterations outside of the anthracene body of the fluorophore have less effects on these kinetics.

3.3. Quantum chemical estimations of radiative and ISC rates from S_1

In order to investigate possible pathways for the IHA effect in the brominated fluorophores, to what extent they can contribute to the ISC rates and relate to the fluorescence rates we performed quantum-chemical calculations. The fluorescence rate (k_r) and the ISC rate (k_{isc}) were calculated for all four dyes, at different levels of density functional theory (DFT) and employing a polarizable continuum model (PCM) to account for solvent effects. Three different DFT/PCM methodologies were employed (TDA/B3LYP/TZP (COSMO), TDA/wB97X/TZP (COSMO) and TDA/B3LYP/TZP (SM12), further described in Supplementary part S3).

Irrespective of which of the methodologies was employed, the fluorescence redshift with higher degree of bromination (figures 4(a)–(c)) was well reproduced in the calculations, together with a slight decrease of the S_1-S_0 oscillator strength for CFl-4Br, further contributing to the lower fluorescence intensities observed for this fluorophore. However, using either of the range-separated wB97X functional with COSMO model or the B3LYP functional with the SM12 model expectedly overestimated the energy of the S_1 state, E(S_1), compared to the results of the B3LYP functional with the COSMO model, which perfectly matched with the experimental data (table 1). At the same time, all methods predicted the position of the T_1 energy level near 1.7 eV (with some exceptions for 4Br, table 3). This, together with the small spin–orbit coupling matrix elements (SOCMEs), S_1 $|\hat{H}_{SO}|T_1$, resulted in very small ISC rates, at a level of 10^2-10^4 s^{-1}. This is three to six orders of magnitude smaller than what was observed in the experiments (figure 5). Moreover, the TDA/B3LYP/TZP (COSMO) methodology couldn´t reproduce the IHA trend for k_{isc} (for CFl-2Br it is smaller than for

Table 3. Energies of lowest lying electronic states (in eV) for CFl, CFl-Br, CFl-2Br, CFl-4Br and FITC, oscillator strengths for the corresponding S_0-S_1 transitions and SOCMEs S_1 $|\hat{H}_{SO}|T_n$ between S_1 state and T_n states (in cm^{-1}). Calculations were performed at S_1 state geometries.

	TDA/B3LYP/TZP (COSMO)				TDA/wB97X/TZP (COSMO)				TDA/B3LYP/TZP (SM12)				
	$E(S_1)$	$E(T_1)$	$f(S_1\text{-}S_0)$	$\mathbf{S_1}\ \mathbf{\lvert\hat{H}_{SO}\rvert T_n}$	$E(S_1)$	$E(T_1)$	$f(S_1\text{-}S_0)$	$\mathbf{S_1}\ \mathbf{\lvert\hat{H}_{SO}\rvert T_n}$	$E(S_1)$	$E(T_1)$	$E(T_2)$	$f(S_1\text{-}S_0)$	$\mathbf{S_1}\ \mathbf{\lvert\hat{H}_{SO}\rvert T_n}$
CFl	2.47 (2.42)[a]	1.77	1.282	0.10	2.66	1.97	1.304	0.03	2.95	1.68	2.61	0.612	0.73 (n = 1) 0.31 (n = 2)
CFl-Br	2.45 (2.37)[a]	1.76	1.367	0.13	2.51	1.71	1.405	0.09	2.92	1.66	2.62	0.693	0.81 (n = 1) 1.29 (n = 2)
CFl-2Br	2.31 (2.34)[a]	1.69	1.271	0.09	2.50	1.71	1.492	0.17	2.91	1.64	2.62	0.851	1.33 (n = 1) 2.18 (n = 2)
CFl-4Br	2.11 (2.30)[a]	1.57	0.841	0.69	2.54	1.89	1.255	0.11	2.34	1.47	2.28	0.178	1.92 (n = 1) 1.03 (n = 2)
FITC	2.37	1.70	1.074	0.14	2.61	1.93	1.252	0.04	2.73	1.64	2.56	0.347	0.50 (n = 1) 0.49 (n = 2)

[a] Experimental emission maxima.

Table 4. Fluorescence and ISC rates (k_r and k_{isc}) calculated at different levels of TDDFT versus experimental estimations.

	TDA/B3LYP/TZP (COSMO)		TDA/wB97X/TZP (COSMO)		TDA/B3LYP/TZP (SM12)			Exp
	k_r, s^{-1}	k_{isc} (S_1−T_1), s^{-1}	k_r, s^{-1}	k_{isc} (S_1−T_1), s^{-1}	k_r, s^{-1}	k_{isc} (S_1−T_1), s^{-1}	k_{isc} (S_1−T_2), s^{-1}	k_{isc}, s^{-1}
CFl	3.4×10^8	2.4×10^4	4.0×10^8	2.4×10^3	1.6×10^8	1.2×10^2	3.4×10^7	1.08×10^7
CFl-Br	3.6×10^8	4.4×10^4	3.8×10^8	1.0×10^4	2.0×10^8	1.6×10^2	7.7×10^8	9.45×10^7
CFl-2Br	2.9×10^8	3.4×10^4	4.1×10^8	3.7×10^4	3.1×10^8	3.9×10^2	2.4×10^9	3.09×10^8
CFl-4Br	1.6×10^8	7.0×10^6	3.5×10^8	4.1×10^4	4.2×10^7	5.5×10^5	5.2×10^9	8.93×10^8
FITC	2.6×10^8	5.8×10^4	3.7×10^8	4.4×10^3	1.1×10^8	1.3×10^3	5.7×10^8	9.60×10^6

CFl-1Br). The main reason for the small values of k_{isc} for the S_1-T_1 channel, irrespective of the level of theory used, is the very large S_1-T_1 energy gap. A second major reason is that both the S_1 and T_1 states correspond to $\pi\pi^*$ electronic states, without any significant contribution from natural transition orbitals (NTOs) of the Br atoms (See SI, table S1). Thus, the resulting S_1 $|\hat{H}_{SO}|$ T_1 SOCMEs are quite small at both TDA/B3LYP/TZP (COSMO) and TDA/wB97X/TZP (COSMO) levels. Within the TDA/B3LYP/TZP (SM12) approach S_1 $|\hat{H}_{SO}|$ T_1 reaches 1.92 cm^{-1} for the CFl-4Br tri-anion, which due to the large S_1-T_1 energy gap, however, still does not significantly improve the matching with the experimental data ($k_{isc}(S_1\text{-}T_1)_{theor} = 5.5 \times 10^5$ s^{-1} versus $k_{isc}(S_1\text{-}T_1)_{exp} = 8.4 \times 10^8$ s^{-1} for CFl-4Br).

As a possible explanation to the experimental trends in k_{isc} one may then consider the second lowest triplet state of the fluorophores, T_2, as a possible acceptor state for S_1 deactivation. Both the wB97X and B3LYP functionals with the COSMO solvent model predict the T_2 state to be higher in energy than the S_1 state. This would make S_1-T_2 ISC thermodynamically forbidden. However, TDA/B3LYP/TZP calculations based on electron density distributions within the SM12 model predict a stabilization of the T_2 state that makes it lower in energy than the S_1 state (table 3). This suggests that an additional S_1-T_2 channel for the ISC can be considered. By taking this S_1-T_2 ISC channel into account, we obtain k_{isc} rates which are in reasonable agreement with the experimental results, with deviations between the calculated and experimental data not exceeding one order of magnitude (table 4). The reason for the difference between the COSMO and the SM12 solvent models in this case might originate from the better parametrization of density for the description of multicharged anions by the SM12 model. By orbital nature, the T_2 state corresponds to a $\pi\pi^*$ symmetry, as well as the T_1 and S_1 states.

Thus, the IHA effect, increasing from CFl, over CFl-1Br, CFl-2Br to CFl-4Br, and as directly observed via the measured ISC rates (figure 5), can be correctly reproduced by accounting for the additional channel of S_1-T_2 ISC. In contrast, different computational methodologies only accounting for ISC via an S_1-T_1 channel give considerably underestimated ISC rates compared to the experimental data, largely due to the large S_1-T_1 splitting values. It can be noted that a ISC via a S_1-to-T_2 transition is still consistent with FP studies, in which T_1 state absorption was identified following fluorophore excitation [38], given that a fast T_2-to-T_1 relaxation likely occurs after the S_1-to-T_2 state transition, before recovery to S_0. Such fast T_2-to-T_1 relaxation is also fully consistent with the TRAST measurements, and it would take place within the T state (figure 2(a)), well before its relaxation to S_0 or $\dot{R}^+$.

4. Conclusions

By TRAST experiments, we could directly measure excitation-induced population build-up of triplet and photo-oxidized states in carboxy-fluorescein and in high triplet yield, brominated variants thereof. Bromination was found to generate a prominent internal heavy atom (IHA) enhancement of the intersystem crossing (ISC) rates, and our DFT calculations suggest this ISC to take place via a higher triplet state, followed by relaxation to the lowest triplet state. A corresponding external heavy atom (EHA) enhancement was found upon adding potassium iodide (KI). In contrast to the common view of KI as a fluorescence quencher, addition of KI resulted in lowered triplet state populations in the brominated fluorophores. This can be attributed to much lower relative enhancements of the (intrinsically very prominent) ISC rates, than of the (orders of magnitude lower) triplet decay rates. Together with an antioxidative effect on the fluorophores, KI can thus act as a fluorescence enhancing compound on the brominated fluorophores.

In contrast to SMD and FCS techniques, TRAST experiments do not rely on high signal-to-background conditions, nor on fluorophores with high brightness or a high time resolution. The experiments are therefore broadly applicable, also on biological samples and living cells, and can be performed under more moderate excitation intensities. However, TRAST experiments rely on excitation-induced build-up of fluorophore dark transient states, such as triplet states, in the samples. Therefore, excitation intensities and doses may sometimes reach a level where photo-toxic effects need to be considered. For the very high triplet yield (>90%) fluorophores used here however, much lower excitation intensities are needed in the TRAST

measurements to drive these fluorophores into their triplet states. The photophysical characterization of this work thus suggests TRAST measurements based on high triplet yield fluorophores as a useful approach for biomolecular interaction and sensing studies, with long-lived, highly sensitive dark states of these fluorophores followed under more biologically relevant conditions, for sensing and quenching studies in living cells and biological tissues.

Acknowledgments

This study was supported by the Swedish Research Council (VR 2021-04556, VR OQS 2016-06122), the Swedish Foundation for Strategic Research (SSF BENVAC RMX18-0041), and the Chemical Biology Consortium Sweden (project CBCS0366). The authors also acknowledge Krister Lundgren at the Swedish Metabolomics Centre, Scilifelab, Umeå for the high-resolution MS characterization, as well as the Swedish National Infrastructure for Computing (SNIC 2022-3-34 and NAISS 2023/5-77) at the National Supercomputer Centre of Linköping University (Sweden) partially funded by the Swedish Research Council (VR 2018-05973).

Data availability statement

The data that support the findings of this study are openly available at the following URL/DOI: https://zenodo.org/record/7928614.

Conflicts of interest

The authors have declared that no conflicting interests exist.

ORCID iDs

Baris Demirbay https://orcid.org/0000-0002-5454-7437
Jerker Widengren https://orcid.org/0000-0003-3200-0374

References

[1] Blom H and Widengren J 2017 Stimulated emission depletion microscopy *Chem. Rev.* **117** 7377–427
[2] Ha T and Tinnefeld P 2012 Photophysics of fluorescent probes for single-molecule biophysics and super-resolution imaging *Annu. Rev. Phys. Chem.* **63** 595–617
[3] Widengren J 2010 Fluorescence-based transient state monitoring for biomolecular spectroscopy and imaging *J. R. Soc. Interface* **7** 1135–44
[4] Spielmann T, Xu L, Gad A K, Johansson S and Widengren J 2014 Transient state microscopy probes patterns of altered oxygen consumption in cancer cells *The FEBS Journal* **281** 1317–32
[5] Chmyrov V, Spielmann T, Hevekerl H and Widengren J 2015 Trans–Cis isomerization of lipophilic dyes probing membrane microviscosity in biological membranes and in live cells,' *Anal. Chem.* **87** 5690–7
[6] Tornmalm J, Piguet J, Chmyrov V and Widengren J 2019 Imaging of intermittent lipid-receptor interactions reflects changes in live cell membranes upon agonist-receptor binding *Sci. Rep.* **9** 18133
[7] Nguyen V-N, Kumar A, Lee M H and Yoon J 2020 Recent advances in biomedical applications of organic fluorescence materials with reduced singlet–triplet energy gaps *Coord. Chem. Rev.* **425** 213545
[8] Xu Z *et al* 2022 A biocompatible photosensitizer with a high intersystem crossing efficiency for precise two-photon photodynamic therapy *Materials Horizons* **9** 1283–92
[9] Yang Z *et al* 2021 Incorporating spin–orbit coupling promoted functional group into an enhanced electron DA system: A useful designing concept for fabricating efficient photosensitizer and imaging-guided photodynamic therapy *Biomaterials* **275** 120934
[10] Nguyen V-N *et al* 2020 A thiocoumarin-based turn-on fluorescent probe for hypochlorite detection and its application to live-cell imaging *Sensors Actuators B* **317** 128213
[11] Chen C, Ni X, Tian H W, Liu Q, Guo D S and Ding D 2020 Calixarene-based supramolecular AIE dots with highly inhibited nonradiative decay and intersystem crossing for ultrasensitive fluorescence image-guided cancer surgery *Angew. Chem.* **132** 10094–8
[12] Marian C M 2001 spin–orbit coupling in molecules *Rev. Comput. Chem.* **17** 99–204
[13] Lakowicz J R 2006 *Principles of Fluorescence Spectroscopy* (Springer)
[14] van Amerongen H and van Grondelle R 1995 [9] Transient absorption spectroscopy in study of processes and dynamics in biology *Methods Enzymol.* (Elsevier) vol 246, pp 201–26
[15] Chen E and Chance M R 1993 [6] Nanosecond transient absorption spectroscopy *Methods Enzymol.* **226** 119–47
[16] Widengren J, Mets U and Rigler R 1995 Fluorescence correlation spectroscopy of triplet states in solution: a theoretical and experimental study *J. Phys. Chem.* **99** 13368–79
[17] Widengren J and Schwille P 2000 Characterization of photoinduced isomerization and back-isomerization of the cyanine dye Cy5 by fluorescence correlation spectroscopy *The Journal of Physical Chemistry A* **104** 6416–28
[18] Widengren J and Seidel C A 2000 'Manipulation and characterization of photo-induced transient states of Merocyanine 540 by fluorescence correlation spectroscopy, *Phys. Chem. Chem. Phys.* **2** 3435–41
[19] Widengren J, Dapprich J and Rigler R 1997 Fast interactions between Rh6G and dGTP in water studied by fluorescence correlation spectroscopy *Chem. Phys.* **216** 417–26
[20] Chmyrov A, Sandén T and Widengren J 2010 Iodide as a fluorescence quencher and promoter mechanisms and possible implications *J. Phys. Chem. B* **114** 11282–91
[21] Mets Ü, Widengren J and Rigler R 1997 Application of the antibunching in dye fluorescence: measuringthe excitation rates in solution *Chem. Phys.* **218** 191–8
[22] Widengren J and Mets Ü 2002 Conceptual basis of fluorescence correlation spectroscopy and related techniques as tools in bioscience *Single Molecule Detection in Solution: Methods and Applications* ed J Enderlein, R A Keller and C Zander (Heidelberg: Wiley-VCH) pp 69–120
[23] Widengren J 2023 Transient state (trast) spectroscopy and imaging: exploiting the rich information source of fluorophore dark state transitions *Fluorescence Spectroscopy and Microscopy in Biology* ed R Sachl and M Amaro (Cham, Switzerland: Springer) (*Springer Series on Fluorescence*) 20 (https://doi.org/10.1007/987-3-031-30362-3)
[24] Du Z *et al* 2022 Imaging fluorescence blinking of a mitochondrial localization probe: cellular localization probes turned into multifunctional sensors *J. Phys. Chem. B* **126** 3048–58
[25] Sandén T, Persson G, Thyberg P, Blom H and Widengren J 2007 Monitoring kinetics of highly environment sensitive states of fluorescent molecules by modulated excitation and

time-averaged fluorescence intensity recording *Anal. Chem.* **79** 3330–41
[26] Sandén T, Persson G and Widengren J 2008 Transient state imaging for microenvironmental monitoring by laser scanning microscopy *Anal. Chem.* **80** 9589–96
[27] Tornmalm J and Widengren J 2018 Label-free monitoring of ambient oxygenation and redox conditions using the photodynamics of flavin compounds and transient state (TRAST) spectroscopy *Methods* **140** 178–87
[28] Hevekerl H, Tornmalm J and Widengren J 2016 Fluorescence-based characterization of non-fluorescent transient states of tryptophan–prospects for protein conformation and interaction studies *Sci. Rep.* **6** 35052
[29] Tornmalm J, Sandberg E, Rabasovic M and Widengren J 2019 Local redox conditions in cells imaged via non-fluorescent transient states of NAD (P) H *Sci. Rep.* **9** 15070
[30] Fudala R, Mummert M E, Gryczynski Z, Rich R, Borejdo J and Gryczynski I 2012 Lifetime-based sensing of the hyaluronidase using fluorescein labeled hyaluronic acid *J. Photochem. Photobiol., B* **106** 69–73
[31] Strömqvist J, Chmyrov A, Johansson S, Andersson A, Mäler L and Widengren J 2010 Quenching of triplet state fluorophores for studying diffusion-mediated reactions in lipid membranes *Biophys. J.* **99** 3821–30
[32] Brändén M, Sandén T, Brzezinski P and Widengren J 2006 Localized proton microcircuits at the biological membrane–water interface *Proc. Natl Acad. Sci.* **103** 19766–70
[33] Gerasimova M A *et al* 2020 Fluorescence and photoinduced proton transfer in the protolytic forms of fluorescein: experimental and computational study *Dyes Pigm.* **173** 107851
[34] Slyusareva E, Tomilin F, Sizykh A, Tankevich E Y, Kuzubov A and Ovchinnikov S 2012 The effect of halogen substitution on the structure and electronic spectra of fluorone dyes *Opt. Spectrosc.* **112** 671–8
[35] Ringemann C, Schönle A, Giske A, Von Middendorff C, Hell S W and Eggeling C 2008 Enhancing fluorescence brightness: effect of reverse intersystem crossing studied by fluorescence fluctuation spectroscopy *Chem. Phys. Chem* **9** 612–24
[36] Reindl S and Penzkofer A 1996 Triplet quantum yield determination by picosecond laser double-pulse fluorescence excitation *Chem. Phys.* **213** 429–38
[37] Spielmann T, Blom H, Geissbuehler M, Lasser T and Widengren J 2010 Transient state monitoring by total internal reflection fluorescence microscopy *J. Phys. Chem. B* **114** 4035–46
[38] Korobov V and Chibisov A 1978 Primary processes in the photochemistry of rhodamine dyes *J. Photochem.* **9** 411–24